Switching response of MgB_2 thin-film microwave resonators due to local nonlinear Joule heating

G. Ghigo, R. Gerbaldo, L. Gozzelino, F. Laviano, and E. Mezzetti
Department of Physics, Politecnico di Torino, C.so Duca degli Abruzzi 24, 10129 Torino, Italy
(Received 23 March 2010; revised manuscript received 29 June 2010; published 24 August 2010)

We investigated the switching response of MgB_2 coplanar waveguide resonators to increase of rf currents. A model based on the heat balance equation is able to account for the observed behaviors, including the presence of a thermal bistability regime. The model also reproduces the temperature dependence of the limiting currents. Results are consistent with the hypothesis that a hot spot is formed due to local Joule heating in correspondence with a weak link. Weak links are modeled as long S-N-S junctions, originating from the transition to the normal state of rows of MgB_2 grains. This thermal process is proposed as the main mechanism setting the performance limit of polycrystalline MgB_2 films in microwave applications.

DOI: 10.1103/PhysRevB.82.054520 PACS number(s): 74.25.N−, 74.78.−w, 74.70.Ad, 84.40.Dc

I. INTRODUCTION

Superconducting microwave resonators are widely used devices with a variety of applications in very different fields, ranging from telecommunications to fundamental physics. Recently, the interest for on-chip resonators, such as coplanar waveguide (CPW) resonators, has been renewed since, due to their low internal losses and small transverse dimensions, they are used in the development of quantum circuits,[1] detectors operating at microwave frequencies[2] and other nonlinear devices, such as bifurcation or parametric amplifiers.[3,4]

In this work we investigate the nonlinear (switching) response of magnesium diboride (MgB_2) CPW resonators with the twofold aim to determine the factors limiting their microwave performance—to state the reliability of this material for applications in microwave circuits in the linear regime—and to understand the potential of the material in view of its application in nonlinear devices.

The great interest in MgB_2 from a fundamental point of view is mainly due to its two-gap nature that generates a rich variety of behaviors.[5] However, interpretation of experimental results in real systems can be flawed by the presence of granularity and disorder which give rise to completely different behaviors with respect to the intrinsic ones. Since it is extremely challenging to fully eliminate both of them, investigating the effects of granularity and disorder is a mandatory task also for good-quality materials, in order to meet the strong demand of reliable applications. The main issue to address is the relevance of weak-link (WL) effects in good-quality polycrystalline MgB_2 films. In fact, this is usually excluded because of the relatively large coherence lengths [estimated as $\xi_\pi(0)=51$ nm and $\xi_\sigma(0)=13$ nm for the two bands].[5] Nevertheless, even if polycrystalline MgB_2 can be thought as a set of strongly linked grains, the anisotropy of the main properties, e.g., coherence length and grain critical current density, prevents to consider it as a uniform medium. Thus granularity effects can emerge when critical conditions of temperature,[6] magnetic field,[7] or bias rf current (this work) are approached. In these cases, *weak links* are made of entire grains or rows of grains switched to the normal metallic state. For these reasons, weak links in MgB_2 polycrystalline samples, when present, can be assimilated to proximity superconductor-normal metal-superconductor S-N-S Josephson junctions, in a configuration similar to one described in Ref. 8 for low-T_c transition-edge devices. Actually, granularity has been observed in MgB_2 film and bulk samples when specific experiments have been performed.[9–12]

The presence of WLs in such extreme bias conditions implies a number of behaviors in MgB_2 films carrying microwave signals. In fact, when the resonator is slightly anharmonic for the presence of a nonlinear element at the WL, there will be a bending of the resonance curves as the drive power is increased, which eventually results in hysteretic behavior.[13] This can be interpreted as the effect of nonlinear local Joule heating that develops a hot spot at the WL through the absorption of microwave power. Bifurcation occurs at a critical power and frequency, at the onset of a double-valued resonance curve. At this critical point the oscillator dynamics suddenly develops qualitatively new behavior, changing from one stable state of oscillation to three states of oscillation, one of which is unstable and results in a switching response.[14] This also means that the current carrying capability of the film is limited by self-heating processes rather than by intrinsic critical current or by critical currents determined by pinning or surface barriers.

We investigated the above described phenomenology, i.e., switching response due to the presence of weak-link effects, originating from the increase in rf currents above a given threshold, by means of CPW resonators obtained from MgB_2 thin films. It turns out that this kind of resonant device has sensitivity high enough to detect the switching of a single weak link (or the penetration of a single vortex).[7] A model based on the heat balance equation is able to account for the observed behaviors, including the presence of a regime of thermal bistability. Furthermore, it can be employed to reproduce the temperature dependence of the limiting currents. Results are consistent with the hypothesis of the presence of weak links in the form of long S-N-S junctions, where the barrier is a layer of MgB_2 grains switched to the normal state.

The paper is organized as follows. In Sec. II we give some basic details on samples and experimental techniques. In Sec. III the phenomenology concerning switching response as a function of rf current and temperature is shown and its interpretation as a weak-link-induced effect is discussed. In Sec. IV we introduce a local Joule heating model, showing that the observed behaviors can be well described in terms of

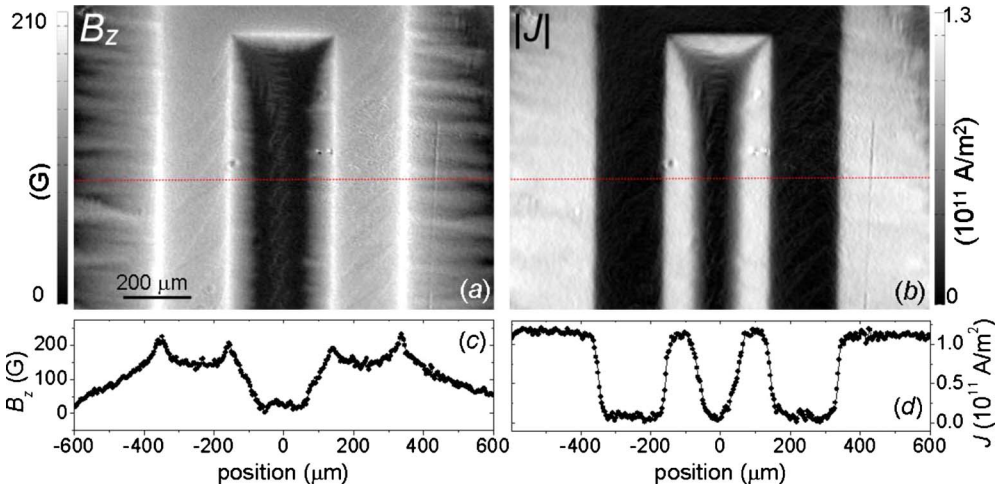

FIG. 1. (Color online) (a) Magnetic field map obtained by magneto-optical imaging of the resonator at $T=3.9$ K and $H_{dc}=75$ Oe. (b) Current-density map obtained by inversion of the field map (see text). (c) Magnetic field and (d) current-density profiles along the dotted lines in (a) and (b), respectively.

a hot spot located at the weak link. Finally, Sec. V summarizes our results.

II. EXPERIMENTAL DETAILS

Half-wavelength coplanar waveguide resonators were obtained by means of photolithographic and ion-milling processes from MgB_2 films grown on sapphire substrates by a coevaporation technique followed by *in situ* annealing.[12,15] The representative device that has been selected for the present study is 140 nm thick and is covered by a 35-nm-thick Au layer, reproducing the same pattern of the superconducting resonator (including the ground planes). The length of the central conductor is 8 mm, its width is 300 μm, and its distance to the ground planes is 200 μm. A detail of the resonator, including an open end of the central conductor and part of the ground planes, can be seen in Fig. 1, where a magneto-optical picture is shown. Magneto-optical imaging (MOI) with indicator film is a powerful tool to visualize the magnetic field distribution and we routinely use it to check the quality and real homogeneity of the produced resonators. Moreover, exploiting a model-independent inversion technique,[16] we can obtain the map of the local current density, j [Fig. 1(b)] from the map of the local induction [Fig. 1(a)], when a given dc magnetic field is imposed. The j map can in turn be used to estimate the dc critical current density, j_c^{dc}. Figure 1(c) shows that, for an imposed dc field of 75 Oe, the induction profile is that typical for the Bean model and, accordingly, Fig. 1(d) shows current density plateaus corresponding to vortex-penetrated regions, where a critical state develops with $j=j_c^{dc}=1.1\times10^{11}$ A/m^2. This value is comparable to high transport j_c measured in optimal MgB_2 films on sapphire substrates.[17]

Concerning the microwave characterization of the resonator, we used a vector network analyzer to acquire the complex transmission coefficient, S_{21}, as a function of the driving frequency, f, in the gigahertz range. Resonance curves were measured at different values of temperature (by using a He-flow cryostat) and rf power (in the range from −40 to 8 dBm), in zero dc magnetic field. Figure 2 shows a typical superconducting transition: effective surface resistance and reactance were evaluated from resonance frequency and quality factor by the method described in Ref. 15, for a sample without Au coating (the inset shows an example of the resonance measured in the linear regime fitted by a Lorentzian curve). The introduction of an Au layer on top of the resonator is aimed at better investigating the effects of local Joule heating (resulting in discontinuities in the response) by reducing the effects of global heating (overall distortion of the resonance curves) through an increased heat conductance.[18] In fact, the Au coating provides an additional channel for heat diffusion. This technique is used, for instance, to avoid or to inhibit the nucleation of thermomagnetic instabilities generating vortex avalanches in MgB_2

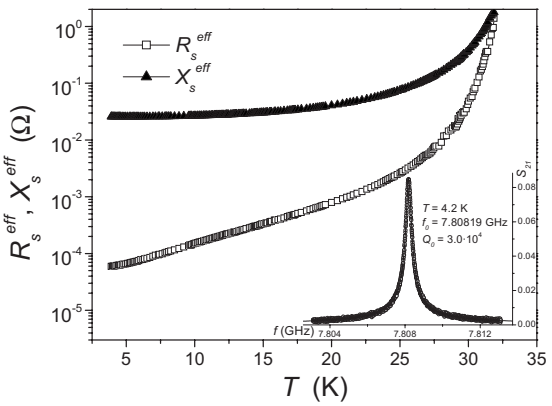

FIG. 2. Surface resistance, R_s^{eff}, and reactance, X_s^{eff}, as a function of temperature, as obtained from central frequency and quality factor of resonance curves for a device without Au top layer, by the method described in Ref. 15. R_s^{eff} and X_s^{eff} are effective values since dielectric losses were not taken into account (the correction is of the order of the residual resistance, significantly affecting only low-temperature data). The inset shows the resonance at $T=4.2$ K, fitted by a Lorentzian curve.

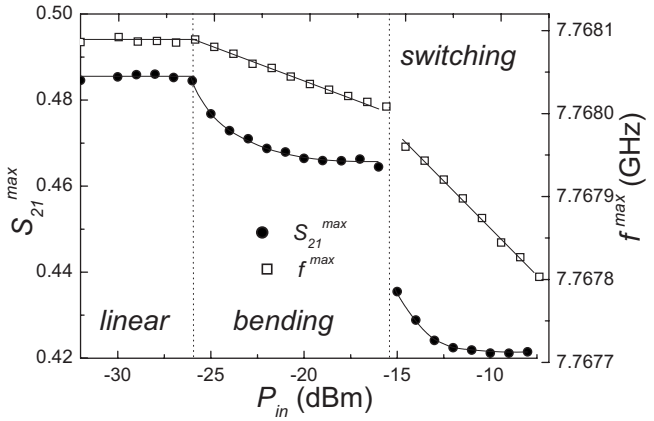

FIG. 3. Dependence of the maximum scattering parameter S_{21} (left scale) and of the corresponding frequency (right scale) on the input microwave power, at $T=5$ K. The graph is divided into three regions, depending on the observed regime: (i) linear (Lorentzian resonance curves); (ii) bending (slightly deformed resonance curves), and (iii) switching (bistability). In the latter case, reported values relate to the maximum of the lower curve, between the jumps (see figures below).

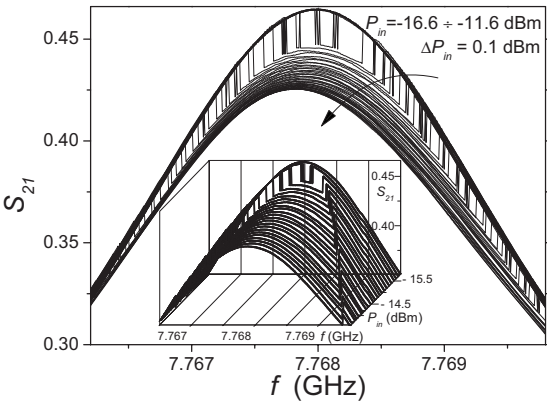

FIG. 4. Resonance curves for different values of input power, P_{in}, in the switching regime, at $T=5$ K. First curves perfectly collapse and the first one showing switching is that for $P_{in}=-15.7$ dBm. The inset shows a three-dimensional plot of the curves for P_{in} among −15.8 and −13.6 dBm.

films at low temperatures.[19] The thin Au layer we used (thickness 35 nm) is enough to significantly reduce the effects of global heating but it still allows the formation of local hot spots when local critical conditions are reached.[20] On the other hand, we observed a decrease in the quality factors of Au-coated resonators with respect to uncoated ones. This effect is similar to what found in a different configuration (disk resonator) in Ref. 21, where the enhancement of the effective impedance of the resonators by an Au layer was explained by the impedance transformation method.[22]

III. WEAK-LINK SWITCHING

Superconducting CPW resonators buildup large amplitude oscillations near resonance, even for a very weak driving signal. As stated in Sec. I, when anharmonicity is present, e.g., due to a nonlinear Josephson junction element, a distortion of the resonance curve and eventually a hysteretic behavior is expected. At a critical power and frequency (the bifurcation point) the resonance curve becomes double valued and the oscillator develops dynamic bistability.

We observe these effects in our resonators, even without the explicit introduction of an artificial weak link.[18] Figure 3 shows a view of the different regimes observed as a function of the input power, through the coordinates of the resonance curve maxima. At low rf power (linear regime) resonance curves can be fitted by Lorentzian curves, as in the case shown in the inset of Fig. 2. As the power is increased, a slight deformation of the resonance curves sets up ("bending" region in Fig. 3), until finally bistability (double-valued resonance curves) and hysteresis become evident ("switching" region). Since the process concerns only *a part* of the resonator—where the granularity-induced weak link develops—some differences with the effects observed in engineered samples where the weak link crosses the whole resonator are expected. Thus is not surprising that in our resonators the instability nucleates from only slightly deformed resonance curves. Figure 4 shows the resonance curves for different values of input rf power in the switching regime. The curves scale until bistability develops, as in the simulations proposed in Ref. 23 for weak-link switching in $YBa_2Cu_3O_{7-x}$. As the input power increases, the bifurcation point moves away from the central frequency. Concerning this point, it is worthwhile noting that the switching power level moves up (slightly) as the input power increases, exactly as in Ref. 24, where such behavior has been explained in the frame of a thermal effect. As temperature is increased, features gradually vanish (Fig. 5).

Bistability at the bifurcation point in low-temperature conditions can be clearly observed in Fig. 6 (amplitude as a function of time for a given frequency in the instability region) which shows that system oscillates between two states that are well defined and stable with respect to time. The hysteresis connected to the recovery of the first resonance curve once the system has jumped to the second more dissipative characteristic has been described in terms of dissipation (inverse of the unloaded quality factor) vs circulating power in Ref. 18, where it was shown to be consistent with a

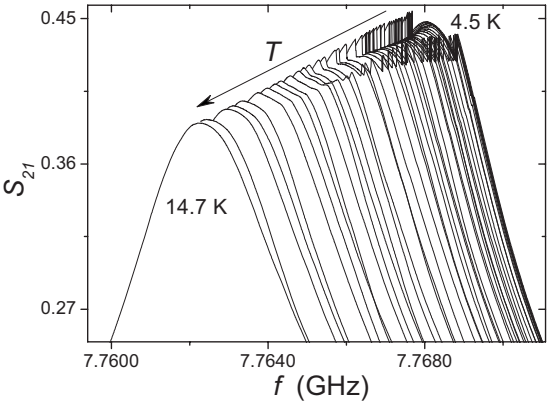

FIG. 5. Resonance curves for different values of temperature at the input power of −15.4 dBm.

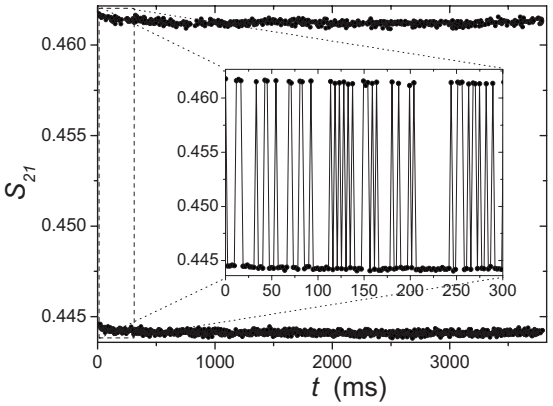

FIG. 6. Scattering parameter S_{21} as function of time for $T=5$ K, $f=7.768$ GHz, and $P_{in}=-15.4$ dBm, i.e., at the middle of the transition from one stable state to the other one, more dissipative. The inset shows a magnification of first data, up to 300 ms.

heating effect (accordingly, it was reported that hysteresis in proximity superconductor-normal metal-superconductor Josephson junctions is governed by overheating of the normal metal).[25]

If the features observed in S_{21} are due to the presence of a weak link, both the resistive and the reactive parts of the impedance should be affected by the switching. In fact, the magnitude of S_{21} implicitly contains both of them. Following Ref. 26 and considering the switching response as a small deviation from the linear case, we can write $\Delta R_s \sim \Delta\mathrm{Re}(S_{21}^{-1})$ and $\Delta X_s \sim \Delta\mathrm{Im}(S_{21}^{-1})$, where $\Delta\mathrm{Re}(S_{21}^{-1})$ and $\Delta\mathrm{Im}(S_{21}^{-1})$ are the differences of the values obtained for two input powers, one just below and the other one just above the switching threshold. ΔR_s and ΔX_s are the resistive and reactive parts of the switching contribution to the overall response. In the lower part of Fig. 7 we report such contributions for the case shown in the top panel in terms of S_{21} magnitude. It turns out, as expected for a WL, that switching

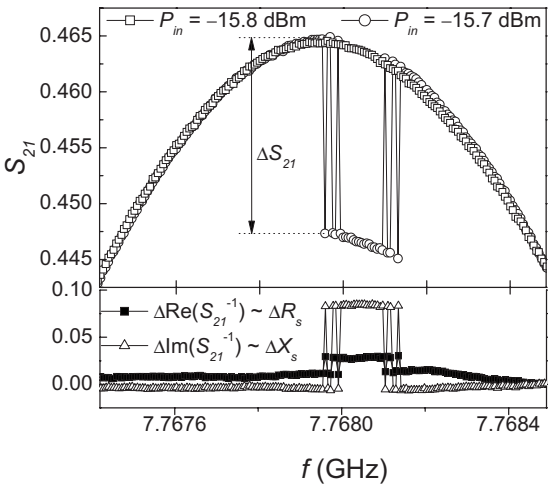

FIG. 7. Resonant curves for two input powers, one just below ($P_{in}=-15.8$ dBm) and the other one just above (-15.7 dBm) the WL-switching threshold ($T=5$ K, top frame). The lower frame shows the increments of the real and imaginary parts of S_{21}^{-1}, as the difference between the values obtained with the two input powers.

contributes both to the resistive and to the reactive parts of the signal.

In summary, a number of evidences—e.g., instability, hysteresis, dissipation, reactance—points to the conclusion that the observed effects are due to the formation of a hot spot in correspondence with a weak link. In order to give further support to this model, we can evaluate the switching energy scale and compare this value to that expected for a reasonable weak link in MgB_2 thin films.

The rf current circulating in the resonator at the switching event, I_{rf}, can be obtained from resonance curves showing the discontinuity close to the curve maximum since in this case[27]

$$I_{\mathrm{rf}} = \sqrt{\frac{4S_{21}^{\max} Q_L P_{in}}{\pi Z_0}}.$$

If the Q_L and $S_{21}^{\max}$ values are obtained by fitting the curve shown in Fig. 7, excluding the down-switched data, a current of 35.4 mA can be estimated. This corresponds to a current density of about 6×10^9 A/m^2 at the resonator edges (where presumably the switching WL is placed), obtained by taking into account the current distribution in the adopted CPW resonator geometry.[28] The energy scale involved in the switching can be estimated through the I_cR_n product that in turn can be calculated from the variation in the output voltage, ΔV_{out}. At the resonance (impedance of the line $Z_0 \approx 50\ \Omega$), $I_cR_n=\Delta V_{out}=V_{in}\Delta S_{21}\approx(P_{in}Z_0)^{1/2}\Delta S_{21}$. In the case shown in Fig. 7, $I_cR_n=813\ \mu$V. If we make the hypothesis that the weak link can be treated as a long S-N-S junction, where the barrier is a row of grains switched to the normal state, the energy scale that sets the I_cR_n product is not related to the energy gap, Δ, but to the Thouless energy $E_{Th}=\hbar D/L^2$, where D is the electronic diffusivity and L is the junction length ($E_{Th}<\Delta$, for long S-N-S junctions). Numerical solutions of the Usadel equation for the whole range of Matsubara frequencies were given in Ref. 29 and can be used to estimate the main parameters. If we consider for Δ the π-gap value ($\Delta_\pi\approx2$ meV), $eI_cR_n/\Delta_\pi\approx0.4$ and, from Ref. 29, $E_{Th}/\Delta_\pi\approx0.08$. This gives $D_\pi\approx2.8\times10^{-3}$ m^2/s and $\xi=\sqrt{\hbar D_\pi/2\Delta_\pi}\approx20$ nm, if L is set to the order of magnitude of grain dimension as evaluated by atomic force microscopy and field emission scanning electron microscopy analysis (not reported) in films without Au coating, $L\approx100$ nm. Since these estimations seem quite reasonable, we conclude that data are consistent with a S-N-S junction model, where the junction barrier is formed by a layer of grains in the normal metallic state.

IV. MODELING THE LOCAL JOULE HEATING EFFECTS

The hypothesis expressed in the previous paragraph, i.e., that the observed instability has a thermic origin (hot-spot formation in correspondence to a WL), can be confirmed by a proper theoretical model. We consider the condition of steady-state heat balance for homogeneous states in the film,[14] $P_J(T,j)=W(T)$, where P_J is the power of the Joule heat release, $W(T)$ is the heat flux from the conductor to the coolant, $W(T)=h(T^p-T_0^p)/d$, $h(T)$ is the heat-transfer coeffi-

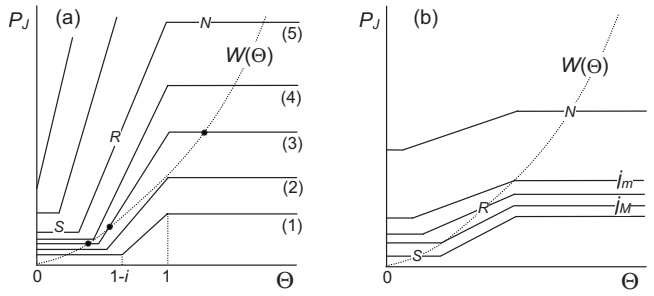

FIG. 8. Graphic solution for the heat balance equation in the case of three intersection points for a single P_J curve (a) and single intersection points (b). The labels *S*, *R*, and *N* indicate the parts of the curves corresponding to the nondissipative, resistive, and normal states of the weak link, respectively.

cient, d is the ratio between the area and the perimeter of the specimen cross section, p is an exponent depending on the cooling conditions, and T_0 is the coolant temperature. A precondition for the existence of a steady-state solution is $d \ll d_c \sim \kappa/h$, where κ is the thermal conductivity. For a superconducting film (h mainly determined by the Kapiza resistance at the interface with the substrate) Gurevich and Mints estimated $d_c \approx 10^{-4}$ m.[14] Since we have $d \approx 7 \times 10^{-8}$ m, the precondition for steady-state heat balance is fulfilled. The stability of such homogeneous states is then guaranteed when $\partial W/\partial T > \partial P_J/\partial T$. Thermal instability arises when the $P_J(T,j)$ and $W(T)$ curves have three intersection points since for one of them the stability criterion cannot hold. This is sketched in Fig. 8(a), in terms of $P_J(\Theta,j)=\rho(\Theta)j^2$ curves, where the dimensionless temperature $\Theta=(T-T_0)/(T_c-T_0)$ has been introduced, with the resistivity $\rho(\Theta)$ sharply depending on Θ in a narrow interval, as expected for the transition of the WL to the normal state. In this case, T is the temperature of the hot spot at the WL while the rest of the film can be considered close to the temperature of the coolant, T_0. Curves from (1) to (5) correspond to increasing values of the circulating current density. Curve (5) shows how the power released to the film changes slope as a function of temperature when the WL passes from the superconducting state, *S* [note that $i=j/j_c(T_0)$], to the resistive, *R*, and finally to the normal state, *N*. Only curves in between (2) and (4), obtained for current densities between j_* and j^*, respectively, can display three intersection points, as shown for curve (3). In this case, the central intersection represents an instable solution, since $\partial W/\partial\Theta < \partial P_J/\partial\Theta$. Curves for $j<j_*$ [for example, curve (1)] have only one stable solution for the WL in the superconducting state and curves for $j>j^*$ [for example, curve (5)] have only one stable solution for the WL in the normal state. When the film temperature is increased above a threshold, the bistability disappears since always $\partial W/\partial\Theta > \partial P_J/\partial\Theta$ [see Fig. 8(b)]: a unique solution is possible, with the WL in the superconducting, or resistive or normal state. The observed temperature threshold is about 9.7 K.

The minimum normal-zone existence current,[14] j_m, can be defined in both the situations from the condition $P_J(T_c,j_m)=W(T_c)$ at $\Theta=1$, that gives

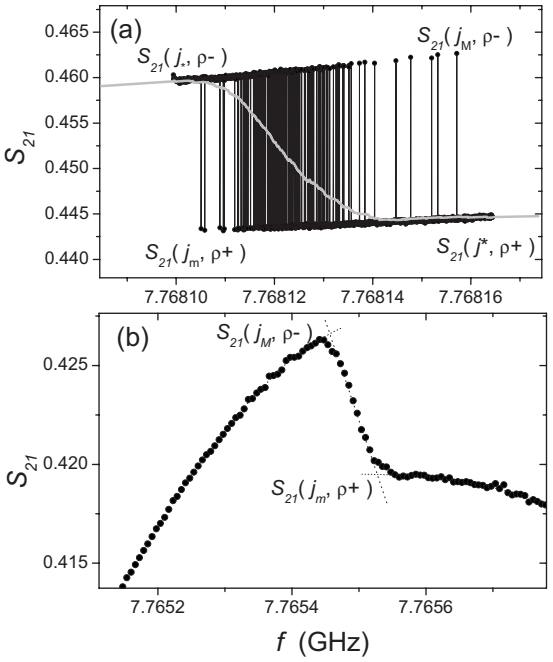

FIG. 9. Transition from the superconducting to the normal state of a weak link (a) in the case of thermal instability at $T=5.0$ K and (b) in the case of smooth transition at $T=11.12$ K. The graphs show the S_{21} values corresponding to the parameters discussed in the text. In panel (a) the average curve is shown in gray.

$$j_m = \left[\frac{h(T_c)T_c^p}{\rho(T_c)d}\right]^{1/2}\left[1-\left(\frac{T_0}{T_c}\right)^p\right]^{1/2}, \tag{1}$$

j_m can be identified with j_* when the conditions for thermal bistability are fulfilled [see curve (2) in Fig. 8(a)]. The maximum superconducting-zone existence current, j_M, can be obtained from the conditions $P_J(T^*,j_M)=W(T^*)$ and $\Theta=1-i$, giving the expressions

$$j_M = \left[\frac{h(T^*)T_c^p}{\rho(T^*)d}\right]^{1/2}\left[\left(\frac{T^*}{T_c}\right)^p-\left(\frac{T_0}{T_c}\right)^p\right]^{1/2}, \tag{2}$$

$$T^* = T_0 + \left[1-\frac{j_M}{j_c(T_0)}\right](T_c-T_0). \tag{3}$$

j_M corresponds to the higher bistability threshold, j^*, when the instability exists [see curve (4) in Fig. 8(a)]. In following the resonance curve during the frequency sweep, the current circulating into the resonator varies over several orders of magnitude, eventually covering also the (j_*-j^*) bistability interval, if existing. The transition of the WL corresponds to a jump in $\rho(T)$ from $\rho-=\rho(T\le T^*)$ to $\rho+=\rho(T_c)$ and a consequent jump in P_J and in the microwave response, as shown in Fig. 9(a). In fact, resonance curves show thermal-bistability oscillations only at low temperature, when the high-quality factor allows large circulating rf currents, whereas at temperatures higher than about 9.7 K the transitions of the WL to and from a higher dissipation state are smooth [Fig. 9(b)]. Figure 9 shows the S_{21} points corresponding to the currents and resistivities of Eqs. (1) and (2),

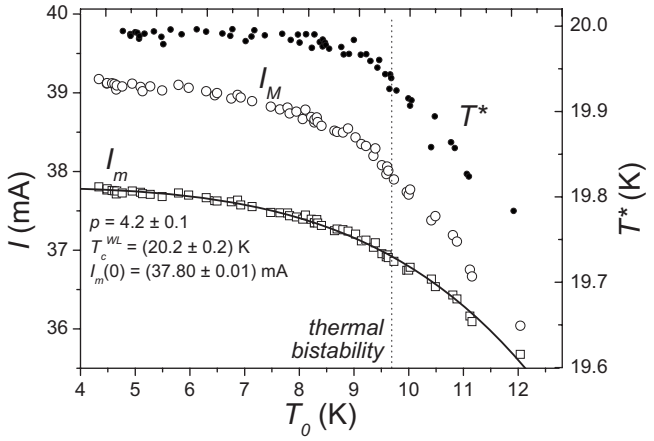

FIG. 10. Minimum normal-zone existence current I_m and maximum superconducting-zone existence current I_M as a function of temperature. I_m is fitted by Eq. (1) (solid line, fitting parameters reported in the graph). The WL temperature T^* (right scale) was obtained by the procedure described in the text.

both in the case of (a) thermal bistability and (b) when the WL transition is smooth.

The currents I_m and I_M, corresponding to the flux of the current density vectors j_m and j_M through the cross section (the nonhomogeneous rf current distribution has to be taken into account),[28] are then deduced from the resonance curves for the whole temperature range. I_m is well fitted by means of Eq. (1) (see Fig. 10) with the parameters reported in the graph. In particular, $p \approx 4$ is consistent with the Kapitza resistance at the metal film–substrate interface[14,30] (in this case, the WL can be cooled also by the rest of the MgB_2 film). T_c represents the critical temperature of the weak link.

Combining Eqs. (1) and (2),

$$T^* = \left[T_0^p + \left(\frac{\rho -}{\rho +} \right) \left(\frac{j_M}{j_m} \right)^2 (T_c^p - T_0^p) \right]^{1/p} \tag{4}$$

if the heat-transfer coefficient h is considered practically constant in the temperature interval $T^* - T_c$. Since $\rho -/\rho + = (j_m/j_*)^2 = (j^*/j_M)^2 \approx [S_{21}(j_m;\rho +)/S_{21}(j_*;\rho -)]^2 \approx 0.93$ [see Fig. 9(a)], the hot-spot temperature T^* can be calculated by means of Eq. (4) in the whole coolant-temperature range (Fig. 10). T^* can be in turn substituted into Eq. (3) to obtain $j_c(T_0)$. It results $j_c(4\ \mathrm{K}) = 4.5 \times 10^{11}\ \mathrm{A/m^2}$, to be compared to $j_m(4\ \mathrm{K}) = 6 \times 10^9\ \mathrm{A/m^2}$. This j_c value is of the same order of magnitude of j_c^{dc} evaluated from MOI (see Fig. 1), not too far from the upper limit—the pair-breaking current—that for MgB_2 is as high as $3 \times 10^{12}\ \mathrm{A/m^2}$.[31] Therefore, even though the rf critical current is *potentially* close to the dc value, the rf current needed for the formation of a hot spot and of the corresponding nonlinearity is *in fact* much lower. This result could be interpreted as follows: when a weaker region of the MgB_2 film (e.g., a defect or a grain boundary or a weaker grain) absorbs microwave power and starts heating up, it leads a number of MgB_2 grains to switch to their normal state, forming the normal barrier of a S-N-S long junction. Note that in the coplanar layout, currents are forced to flow in a narrow region along the resonator edge and therefore cannot avoid the barrier. This process is self-sustaining (more absorption implies more heating, more grains switching to the normal state, and in turn more absorption), up to the formation of a hot spot and to thermal instability, with the effects described above. On the basis of this arguments, the value $j_m(4\ \mathrm{K}) = 6 \times 10^9\ \mathrm{A/m^2}$, about two orders of magnitude lower than the critical one, confirms that the main mechanism limiting the resonator power handling capability is indeed local Joule heating.

V. CONCLUSIONS

The use of coplanar waveguide resonators turned out to be very useful in the study of the mechanisms determining the performance limits of MgB_2 films in microwave applications. In fact, the high sensitivity of such resonant devices to switching of single junctions was demonstrated. This was possible also because of the deposition of an Au top layer, reducing the effects of global heating.

By means of this technique, we were able to investigate thermal bistability phenomena occurring in polycrystalline films due to local Joule heating effects. A simple model based on the formation of a hot spot in correspondence with a weak link can account for the observed dependence of the limiting currents on temperature. The properties of such weak links in good quality polycrystalline MgB_2 films carrying rf currents have been discussed: it turns out that they are made of rows of entire grains, transverse to the current flow direction, switched to their normal metallic state, and can thus be modeled as proximity long S-N-S junctions. With this respect, they are qualitatively different from weak links in the cuprates, which form at the grain boundaries. Accordingly, the estimated critical current density for such "weak links" is on the order of dc j_c ($\approx 4.5 \times 10^{11}\ \mathrm{A/m^2}$). Nevertheless, the effective upper limit for the microwave current density (onset of strong nonlinearity) is significantly lower (about two orders of magnitude), due to the occurrence of heating phenomena. This leads to the conclusion that the rf-current-carrying capability of the film is mainly limited by local self-heating processes rather than by intrinsic critical current or by critical currents determined by disorder (pinning) or geometry (surface barriers). The same should hold for other metallic superconducting materials.[14]

ACKNOWLEDGMENTS

We thank Eugenio Monticone and Chiara Portesi for providing the MgB_2 films and Bruno Minetti for helpful discussions. We gratefully acknowledge financial support from the Italian Ministry of University and Research (MIUR) under the national program PRIN Project No. 2007AW2K4Y.

[1] A. Wallraff, D. I. Schuster, A. Blais, L. Frunzio, R. S. Huang, J. Majer, S. Kumar, S. M. Girvin, and R. J. Schoelkopf, Nature (London) **431**, 162 (2004).
[2] P. K. Day, H. G. LeDuc, B. A. Mazin, A. Vayonakis, and J. Zmuidzinas, Nature (London) **425**, 817 (2003).
[3] E. A. Tholén, A. Ergül, E. M. Doherty, F. M. Weber, F. Grégis, and D. B. Haviland, Appl. Phys. Lett. **90**, 253509 (2007).
[4] B. Abdo, E. Sergev, O. Shtempluck, and E. Buks, Appl. Phys. Lett. **88**, 022508 (2006).
[5] V. Moshchalkov, M. Menghini, T. Nishio, Q. H. Chen, A. V. Silhanek, V. H. Dao, L. F. Chibotaru, N. D. Zhigadlo, and J. Karpinski, Phys. Rev. Lett. **102**, 117001 (2009).
[6] P. Mazzetti, C. Gandini, A. Masoero, M. Rajteri, and C. Portesi, Phys. Rev. B **77**, 064516 (2008).
[7] G. Ghigo, R. Gerbaldo, L. Gozzelino, and F. Laviano (unpublished).
[8] J. E. Sadleir, S. J. Smith, S. R. Bandler, J. A. Chervenak, and J. R. Clem, Phys. Rev. Lett. **104**, 047003 (2010).
[9] N. Khare, D. P. Singh, A. K. Gupta, S. Sen, D. K. Aswal, S. K. Gupta, and L. C. Gupta, J. Appl. Phys. **97**, 076103 (2005).
[10] M. Bar-Sadan, G. Leitus, and S. Reich, J. Supercond. **17**, 497 (2005).
[11] A. J. Purnell, L. F. Cohen, H. Y. Zhai, H. M. Christen, M. P. Paranthaman, D. H. Lowndes, L. Hao, and J. C. Gallop, Supercond. Sci. Technol. **17**, 681 (2004).
[12] G. Ghigo, G. A. Ummarino, R. Gerbaldo, L. Gozzelino, F. Laviano, and E. Mezzetti, Phys. Rev. B **74**, 184518 (2006).
[13] E. A. Tholén, A. Ergül, K. Stannigel, C. Hutter, and D. B. Haviland, Phys. Scr. **T137**, 014019 (2009).
[14] A. V. Gurevich and R. G. Mints, Rev. Mod. Phys. **59**, 941 (1987).
[15] G. Ghigo, D. Botta, A. Chiodoni, L. Gozzelino, R. Gerbaldo, F. Laviano, E. Mezzetti, E. Monticone, and C. Portesi, Phys. Rev. B **71**, 214522 (2005).
[16] F. Laviano, D. Botta, A. Chiodoni, R. Gerbaldo, G. Ghigo, L. Gozzelino, S. Zannella, and E. Mezzetti, Supercond. Sci. Technol. **16**, 71 (2003).
[17] X. Zeng, A. V. Pogrebnyakov, A. Kotcharov, J. E. Jones, X. X. Xi, E. M. Lysczek, J. M. Redwing, S. Xu, Qi Li, J. Lettieri, D. G. Schlom, W. Tian, X. Pan, and Z.-K. Liu, Nature Mater. **1**, 35 (2002).
[18] G. Ghigo, R. Gerbaldo, L. Gozzelino, F. Laviano, G. Lopardo, E. Monticone, C. Portesi, and E. Mezzetti, Appl. Phys. Lett. **94**, 052505 (2009).
[19] E.-M. Choi, V. V. Yurchenko, T. H. Johansen, H.-S. Lee, J. Y. Lee, W. N. Kang, and S.-I. Lee, Supercond. Sci. Technol. **22**, 015011 (2009).
[20] Accordingly, we observed an enhancement of the field threshold for the formation of thermomagnetic instabilities in measurements as a function of dc magnetic field (not shown). The noncomplete inhibition of vortex avalanches for the adopted Au-layer thickness means that the coating still allows the formation of local thermic instability.
[21] A. G. Zaitsev, R. Schneider, J. Geerk, G. Linker, F. Ratzel, and R. Smithley, Appl. Phys. Lett. **75**, 4165 (1999).
[22] N. Klein, H. Chaloupka, G. Müller, S. Orbach, H. Piel, B. Roas, L. Schultz, U. Klein, and M. Peiniger, J. Appl. Phys. **67**, 6940 (1990).
[23] J. Wosik, L. M. Xie, R. Grabovickic, T. Hogan, and S. A. Long, IEEE Trans. Appl. Supercond. **9**, 2456 (1999).
[24] J. Wosik, L. M. Xie, and R. Grabovickic, Supercond. Sci. Technol. **22**, 105003 (2009).
[25] H. Courtois, M. Meschke, J. T. Peltonen, and J. P. Pekola, Phys. Rev. Lett. **101**, 067002 (2008).
[26] T. Jacobs, B. A. Willemsen, and S. Sridhar, Rev. Sci. Instrum. **67**, 3757 (1996).
[27] B. Avenhaus, A. Porch, M. J. Lancaster, and S. Hensen, IEEE Trans. Appl. Supercond. **5**, 1737 (1995).
[28] I. B. Vendik and O. G. Vendik, *High Temperature Superconductor Devices for Microwave Signal Processing—Part II* (Sclanden, St. Petersburg, 1997).
[29] P. Dubos, H. Courtois, B. Pannetier, F. K. Wilhelm, A. D. Zaikin, and G. Schön, Phys. Rev. B **63**, 064502 (2001).
[30] A. V. Sergeev, Phys. Rev. B **58**, R10199 (1998).
[31] T. Dahm and D. J. Scalapino, Appl. Phys. Lett. **85**, 4436 (2004).